

Rec-RIR: Monaural Blind Room Impulse Response Identification via DNN-based Reverberant Speech Reconstruction in STFT Domain

Pengyu Wang and Xiaofei Li

Abstract—This paper presents Rec-RIR for monaural blind room impulse response (RIR) identification. Rec-RIR is developed based on the convolutive transfer function (CTF) approximation, which models reverberation effect within narrow-band filter banks in the short-time Fourier transform domain. Specifically, we propose a deep neural network (DNN) with cross-band and narrow-band blocks to estimate the CTF filter. The DNN is trained through reconstructing the noise-free reverberant speech spectra. This objective enables stable and straightforward supervised training. Subsequently, a pseudo intrusive measurement process is employed to convert the CTF filter estimate into RIR by simulating a common intrusive RIR measurement procedure. Experimental results demonstrate that Rec-RIR achieves state-of-the-art performance in both RIR identification and acoustic parameter estimation. Open-source codes are available online at <https://github.com/Audio-WestlakeU/Rec-RIR>.

Index Terms—System identification, room impulse response, acoustic parameters, convolutive transfer function, deep learning

I. INTRODUCTION

Room impulse response (RIR) models the complete propagation process of sound and contains key information of the acoustic environment. Accurate RIR estimation facilitates a wide range of applications, such as speech enhancement [1], speech recognition [2] and augmented/virtual reality [3]. A common intrusive method for measuring RIR is to play a known excitation signal, such as a maximum length sequence or a sine sweep signal, and then perform inverse filtering on the observation [4], [5]. However, intrusive measurement is expensive and not always practical in real-world applications. In contrast, blind RIR identification aims to estimate normalized RIRs solely from observation of a specific form (e.g., reverberant speech) without known source signals [6], [7], [8].

Deep neural network (DNN)-based blind RIR identification use data-driven methods to learn normalized RIRs directly. Many DNN-based approaches encode fixed-length reverberant speech in the time domain and use a decoder to obtain fixed-length RIR estimates. S2IR-GAN [2] uses a generative adversarial network (GAN)-based architecture to estimate the RIR up to 0.25 s. The discriminator network is optimized to differentiate the estimated RIR from the ground truth RIR.

Pengyu Wang is with Zhejiang University and also with Westlake University, Hangzhou, China (e-mail: wangpengyu@westlake.edu.cn). Xiaofei Li is with the School of Engineering, Westlake University, and the Institute of Advanced Technology, Westlake Institute for Advanced Study, Hangzhou, China (e-mail: lixiaofei@westlake.edu.cn).

Xiaofei Li: corresponding author.

Estimating RIR in the time domain remains challenging due to its long taps, which typically consist of thousands of samples. In FiNS [9], the RIR is decomposed into three distinct components: the direct-path impulse, early reflections and decaying filtered noise signals. A time-domain encoder-decoder architecture is employed to learn both the early RIR and the noise filter, which significantly reduces the output dimension, thus alleviating the difficulty of estimating long RIRs. SG-RIR [10] employs a segmental network that generates one segment of the complete RIR each time, with the network architecture shared across all segments. According to the convolutive transfer function (CTF) approximation [11], the reverberation effect can be modeled within narrow-band filter banks in the short-time Fourier transform (STFT) domain. Therefore, the estimation of long RIR can be replaced by estimating a much shorter CTF filter in the STFT domain, thus simplifying the task. BUDDy [12] and VINP [13] estimate RIRs by implicitly reconstructing the reverberant spectra. Both of them estimate the clean speech and the filter simultaneously and iteratively in STFT domain based on the signal model and DNN predictions.

This work presents Rec-RIR for monaural blind RIR identification. The basis of Rec-RIR is the CTF approximation, which models the reverberation effect within narrow-band filtering. Rec-RIR comprises two main steps: CTF filter estimation and a pseudo intrusive measurement process. Using SpatialNet [14] and its derivative methods [13], [15], [16] as the backbone, we propose an end-to-end DNN consisting of cross-band and narrow-band blocks for CTF estimation. The proposed DNN outputs a fixed-length CTF filter based on the input of arbitrary length, allowing Rec-RIR to make full use of the long input recording. Since RIR is independent of noise, and reverberant speech is the filtered version of clean speech through RIR, we propose to learn the embeddings of reverberant speech and clean speech in the latent space, and use both to estimate the CTF filter. We use the reconstruction error of the reverberant spectrum as the primary objective for supervised training, and incorporate two auxiliary losses to provide guidance for the learning of embeddings. The objective enables stable and straightforward estimation of the CTF filter and, compared with BUDDy and VINP, allows the network to directly estimate the CTF filter without iteration. Further, a pseudo intrusive measurement process is introduced to convert the CTF filter into RIR by simulating a common intrusive RIR measurement procedure, as proposed in [13]. Experimental results demonstrate that Rec-RIR can accurately estimate RIRs and achieves state-of-the-art (SOTA) perfor-

mance in the estimation of acoustic parameters, including reverberation time (RT60), direct-to-reverberant ratio (DRR), and clarity (C50).

II. SIGNAL MODEL

In the time domain, the noisy reverberant speech recording $y(n)$ can be modeled as

$$y(n) = x(n) + w(n) = h(n) * s(n) + w(n), \quad (1)$$

where n is the sample index, $x(n)$ and $w(n)$ denote reverberant speech and additive noise, respectively. Reverberant speech $x(n)$ can be expressed as the convolution of clean speech $s(n)$ and RIR $h(n)$. Notice that we constrain $s(n)$ to have the delay and gain of the direct-path observation, and constrain $h(n)$ to start with the direct-path impulse, to obtain a unique solution for RIR identification.

According to the CTF approximation [11], in the STFT domain, we have

$$\begin{aligned} Y(f, t) &= X(f, t) + W(f, t) \\ &\approx \sum_{l=0}^{L-1} H_l(f) S(f, t-l) + W(f, t), \end{aligned} \quad (2)$$

where f and t are the indices of frequency band and frame, respectively. $Y(f, t)$, $X(f, t)$, $S(f, t)$ and $W(f, t)$ are the STFT coefficients of $y(n)$, $x(n)$, $s(n)$ and $w(n)$, respectively. $H_l(f)$ is the l th coefficient of the L -order CTF filter at frequency band f . For simplicity, we define $\mathbf{Y}, \mathbf{X}, \mathbf{S}, \mathbf{W} \in \mathbb{C}^{F \times T}$ as the spectra of recording, reverberant speech, clean speech and noise, respectively, and we define $\mathbf{H} \in \mathbb{C}^{F \times L}$ as the entire CTF filter. Then we have

$$\mathbf{Y} = \mathbf{X} + \mathbf{W} \approx \mathbf{H} \circledast \mathbf{S} + \mathbf{W}, \quad (3)$$

where \circledast denotes temporal convolution operation along the frame axis. CTF approximation models the reverberation effect within narrow-band filtering in the STFT domain. Since the approximation error is sufficiently small to be neglected [17], [18], RIR and CTF contain nearly identical information. Thus, we can convert the estimation of the RIR into that of the CTF, thereby shortening the filter and simplifying the problem.

III. PROPOSED METHOD

In Rec-RIR, we propose a DNN to learn the mapping from the input spectrum \mathbf{Y} to the CTF filter estimate $\hat{\mathbf{H}}$. Subsequently, a pseudo intrusive measurement process is introduced to convert the CTF filter estimate $\hat{\mathbf{H}}$ into RIR estimate $\hat{h}(n)$. The workflow of Rec-RIR is illustrated in Fig. 1.

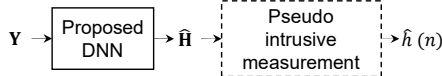


Fig. 1. Workflow of Rec-RIR.

A. Proposed Network

1) *Feature representation:* The input and output features of the proposed DNN are constructed by concatenating the real and imaginary parts of the input spectrum \mathbf{Y} and CTF filter \mathbf{H} along an expanded channel dimension. The input feature is

$$\mathbf{Y}_{ft} = [\text{Re}\{\mathbf{Y}\}; \text{Im}\{\mathbf{Y}\}] \in \mathbb{R}^{2 \times F \times T}, \quad (4)$$

and the output feature is

$$\hat{\mathbf{H}}_{ft} = [\text{Re}\{\hat{\mathbf{H}}\}; \text{Im}\{\hat{\mathbf{H}}\}] \in \mathbb{R}^{2 \times F \times L}. \quad (5)$$

Similar to \mathbf{Y}_{ft} , we define $\hat{\mathbf{X}}_{ft}$ and $\hat{\mathbf{S}}_{ft}$ as the features of estimated reverberant spectrum and clean spectrum, respectively. The corresponding inverse transformation is straightforward.

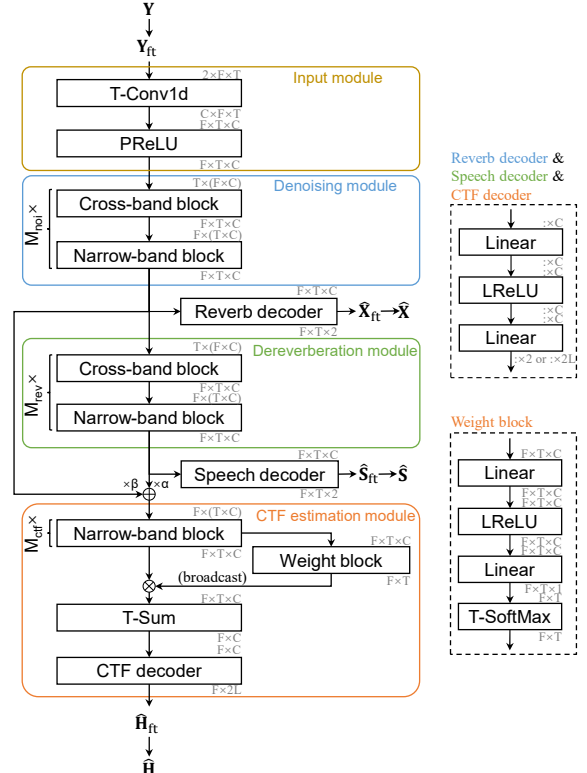


Fig. 2. Architecture of the proposed network.

2) *Modules:* As shown in Fig. 2, the proposed DNN consists of an input module, a denoising module, a dereverberation module, and a CTF estimation module. The input and output sizes are labeled above and below each block, respectively. The reshape and dimension permutation operations are omitted.

Input module This module extracts embeddings from noisy and reverberant recordings. It applies a single 1-D convolutional layer (T-Conv1d) with kernel size 5 and C channels along the frame axis, expanding 2-channel inputs into C -dimensional embeddings per time-frequency (T-F) bin, followed by PReLU activation.

Denoising module and dereverberation module Since RIR is related to reverberation and clean speech but not to noise, we propose denoising and dereverberation modules to learn the embeddings of reverberant speech and clean speech, respectively. Both modules share the same network structure, which reuses the basic architecture from SpatialNet[14] and its extensions[13], [15], and has been proven effective for both denoising and dereverberation tasks. The cross-band block, composed of convolutional layers along the frequency axis and linear layers, processes all frames independently using identical model parameters, and remains consistent with the original design of SpatialNet. Note that as in SpatialNet, the 'F-Linear networks' in cross-band blocks are shared within the denoising module and the dereverberation module, respectively.

However, they are kept separate between these two modules. In general, RIR identification is an offline task. Therefore, we adopt the bidirectional Mamba-based narrow-band block proposed in [13], which consists of stacked one forward Mamba layer and one backward Mamba layer. The narrow-band block processes all frequency bands independently with the same model parameters. The denoising module and the dereverberation module contain M_{noi} and M_{rev} stacked cross-band and narrow-band blocks, respectively. To provide direct guidance for training, we employ two decoders that consist of two linear layers and LeakyReLU activation to transform the output embeddings of both module into reverberant and clean spectra respectively, which require the output embeddings to contain key information of reverberant and clean speech.

CTF estimation module This module takes both reverberant and clean speech embeddings, and outputs the fixed-length CTF filter estimate. Specifically, the outputs of the denoising and dereverberation modules are weighted and summed to form the input of CTF estimation module with learnable weighting parameters α and β . According to the CTF approximation, the narrow-band filter banks across different frequency bands are independent. Therefore, M_{ctf} stacked narrow-band blocks are employed to estimate CTF embeddings. After that, a weight block, which consists of linear layers, LeakyReLU and Softmax activation, is designed to calculate the importance of CTF embeddings at all frames. These weights are distinct for each frequency band. Within each band, the sum of weights along the frame axis equals 1. The weighting mechanism ensures a fixed-length output regardless of the input length, allowing Rec-RIR to accept inputs of arbitrary length and make full use of long input recordings. After weighting, we employ a CTF decoder to transform the CTF embeddings into the CTF filter coefficients. The CTF decoder shares the same structure as the aforementioned decoders, but differs in that it outputs $2L$ dimensions for each T-F bin.

3) *Loss function*: We design a composite loss function for training, which comprises three components: the reconstruction error of reverberant spectrum \mathcal{L}_{rec} , the prediction error of reverberant spectrum \mathcal{L}_{rvb} , and the prediction error of clean spectrum \mathcal{L}_{cln} , which is

$$\mathcal{L} = \mathcal{L}_{\text{rec}} + \lambda_{\text{rvb}} \mathcal{L}_{\text{rvb}} + \lambda_{\text{cln}} \mathcal{L}_{\text{cln}}, \quad (6)$$

where $\mathcal{L}_{\text{rec}} = \mathcal{L}_{\text{RI+Mag}}(\hat{\mathbf{H}} \circledast \mathbf{S}, \mathbf{X})$, $\mathcal{L}_{\text{rvb}} = \mathcal{L}_{\text{RI+Mag}}(\hat{\mathbf{X}}, \mathbf{X})$, $\mathcal{L}_{\text{cln}} = \mathcal{L}_{\text{RI+Mag}}(\hat{\mathbf{S}}, \mathbf{S})$. λ_{rvb} and λ_{cln} are hyperparameters. $\hat{\mathbf{H}}$, $\hat{\mathbf{X}}$ and $\hat{\mathbf{S}}$ are the output of decoders, shown in Fig. 2. $\mathcal{L}_{\text{RI+Mag}}(\cdot, \cdot)$ is defined as [19]

$$\mathcal{L}_{\text{RI+Mag}}(\mathbf{X}, \mathbf{Y}) = \frac{1}{FT} [|||\mathbf{X}| - |\mathbf{Y}|||_1 + ||\text{Re}\{\mathbf{X}\} - \text{Re}\{\mathbf{Y}\}||_1 + ||\text{Im}\{\mathbf{X}\} - \text{Im}\{\mathbf{Y}\}||_1]. \quad (7)$$

Here, \mathcal{L}_{rec} serves as the primary loss, guiding the proposed network to stably learn the direct mapping from the input spectrum to the CTF filter. \mathcal{L}_{rvb} and \mathcal{L}_{cln} act as auxiliary losses, helping the network obtain better hidden representations.

B. Pseudo intrusive measurement process

We employ the pseudo intrusive measurement process proposed in [13] to convert the CTF filter to RIR by simulating a

common intrusive measurement process. Given a logarithmic sine sweep as an excitation signal $e(n)$, there is an inverse filter $v(n)$ that satisfies $e(n) * v(n) = \delta(n)$, where $\delta(n)$ is an impulse [4], [20]. Playing such an excitation signal, according to the signal model, the STFT of noise-free measurement signal is $\mathbf{Z} \approx \hat{\mathbf{H}} \circledast \mathbf{E}$, where \mathbf{E} is the STFT of excitation signal. After all, the RIR is estimated by inverse filtering $\hat{h}(n) = z(n) * v(n)$, where $z(n)$ is the inverse STFT of \mathbf{Z} .

IV. EXPERIMENTS

A. Datasets

We use the same 16 kHz training and test sets as in VINP [13], which are generated by convolving clean speech with RIRs, followed by noise addition.

For training, the clean speech consists of 200 hours of high-quality utterances from DNS Challenge [21] and VCTK [22], as well as the whole EARS [23] corpus. We use 100,000 reverberant and direct-path RIR pairs simulated by gpuRIR [24], in which the speaker and microphone are randomly placed in rooms with dimensions randomly selected within a range of 3 m to 15 m for length and width, and 2.5 m to 6 m for height. Reverberant RIRs have RT60s uniformly distributed within the range of 0.2 s to 1.5 s. To align the clean speech with the recording, we use the direct-path version of the observed signal as the clean speech in our loss function. Direct-path RIRs are generated using the same geometric parameters as the reverberant ones but with an absorption coefficient of 0.99. Noise comes from NOISEX-92 [25] and the training set of REVERB Challenge [26]. The signal-to-noise ratio (SNR) is uniformly distributed within the range of 5 dB to 20 dB.

We use the SimACE test set proposed in [13], in which the microphone recordings are generated by convolving the clean speech from WSJ0 corpus [27] with the downsampled measured RIRs from ACE Challenge [28], and adding noise from the test set in REVERB Challenge with a SNR of 20 dB. During testing, the labels of the acoustic parameters are calculated from the ground truth RIRs.

B. Settings

Before Rec-RIR, the input recordings are normalized using their maximum absolute value. The STFT analysis and synthesis windows are square-root Hann windows with a length of 512 samples and 50% overlap, which means $F = 257$. The numbers of layers are set to $M_{\text{noi}} = 2$, $M_{\text{rev}} = 6$ and $M_{\text{ctf}} = 6$. The dimension of embeddings is set to $C = 96$. The CTF length is set to $L = 60$, which corresponds to RIR estimates with an effective length of approximately 0.96 s. With the above settings, Rec-RIR has 3.1 M parameters and is with 35.2 GMACs/s computational complexity.

For training, we set $\lambda_{\text{rvb}} = 1$ and $\lambda_{\text{cln}} = 1$, segment speech utterances into 4 s, and use 97,092 samples per epoch with a batch size of 4. We adopt the AdamW optimizer [29] and the cosine annealing learning rate scheduler with restarts. The learning rate starts at 0.001 and decays cosinely in each epoch. Training runs for 35 epochs.

In the pseudo intrusive measurement process, we employ the logarithmic sine sweep signal [4], [20] with a frequency

TABLE I
BLIND RIR IDENTIFICATION RESULTS ON SIMACE.

Method	RIR-50 ms		RT60 (s)		DRR (dB)			C50 (dB)			
	RMSE \downarrow	$\bar{\rho}\uparrow$	MAE \downarrow	RMSE \downarrow	$\rho\uparrow$	MAE \downarrow	RMSE \downarrow	$\rho\uparrow$	MAE \downarrow	RMSE \downarrow	$\rho\uparrow$
FiNS [9]	0.067	0.409	0.113	0.167	0.857	2.153	2.639	0.737	6.489	6.597	0.925
BUDDy (pre-trained) [12]	0.054	0.655	0.124	0.173	0.941	3.931	4.570	0.783	4.290	4.654	0.773
BUDDy [12]	0.057	0.621	0.122	0.166	0.952	3.673	4.360	0.774	4.109	4.477	0.779
VINP-TCN+SA+S [13]	0.050	0.695	0.089	0.124	0.934	3.256	3.764	0.872	0.914	1.135	0.961
VINP-oSpatialNet [13]	0.050	0.703	0.103	0.154	0.895	2.398	2.875	0.908	0.977	1.295	0.943
Rec-RIR	0.040	0.805	0.069	0.104	0.994	0.684	0.794	0.994	0.858	1.019	0.978

range of 62.5 Hz to 8000 Hz and a duration of 8.192 s as the excitation signal. Fade-in with 256 samples and fade-out with 128 samples are applied to mitigate spectral leakage.

C. Comparison methods and metrics

We compare Rec-RIR with FiNS [9], BUDDy [12] and VINP [13]. Part of convolutional kernels in FiNS are modified to handle the 16 kHz inputs. For BUDDy, we additionally provide the results using its official pre-trained weights.

We evaluate Rec-RIR using acoustic parameters RT60, DRR and C50. We present their mean absolute error (MAE), root mean square error (RMSE), and Pearson correlation coefficient (ρ). Additionally, we provide RMSE and average ρ ($\bar{\rho}$) of early reflections (marked as RIR-50 ms), corresponding to the 50 ms duration after the direct-path impulse.

D. Results and analysis

As shown in Table I, Rec-RIR achieves the SOTA estimation of the early reflections and the acoustic parameters. The high Pearson correlation coefficients of Rec-RIR indicate stable RIR identification results. Unlike FiNS which learns the early reflections and the noise shaping filters directly from fixed-length inputs, BUDDy, VINP, and Rec-RIR solve the filter in STFT domain based on the spectra of reverberant recordings with arbitrary length. Among these three approaches, the DNNs in BUDDy and VINP do not directly output the filter coefficients. Instead, they alternately update the estimates of clean speech and filters according to the signal model and derive the final estimates after multiple iterations by maximizing likelihood. Differently, Rec-RIR introduces the DNN and loss functions specifically designed for RIR estimation, enabling a direct estimation of CTF filter without the need for any iteration, thus reducing the computational complexity. Fig. 3 shows an example of the estimated RIR, whose ground truth RT60, DRR and C50 are 1.26 s, -1.24 dB and 4.90 dB, respectively. It can be found that Rec-RIR is capable of estimating the impulses in early reflections. The impulses in the measured RIR that occur before 2 ms cannot be fully reconstructed, which is reasonable because we use the direct-path signal as the clean speech. The direct-path signal constrains the time delay and gain of the RIR, resolving the underdetermined problem in RIR identification. However, during training, since the direct-path signal inevitably contains part of frequency response, the estimated RIR may lack the corresponding component. Fig. 4 presents the 2-D projections of the CTF embeddings (before the CTF decoder), where the inputs are derived from the entire test set and the projections are generated using UMAP [30]. As observed, the embeddings

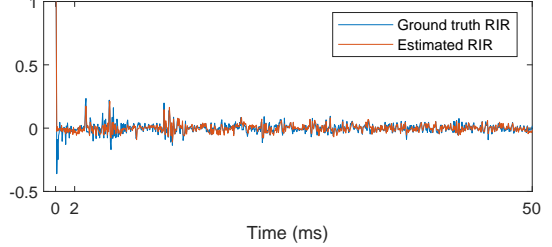


Fig. 3. Example of ground truth and estimated RIRs.

within the latent space exhibit a clear clustering corresponding to the RIR IDs.

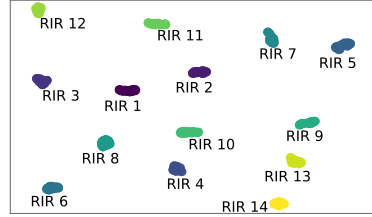


Fig. 4. 2-D projections of CTF embeddings on SimACE.

E. Ablation study

An ablation study with variant loss weights is designed to demonstrate the contribution of the auxiliary losses. We present the mean values and standard deviations of metrics in Table II. Compared with Var-1 which estimates the CTF filter directly using the primary loss, other experiments have lower errors, indicating that both auxiliary losses contribute to the final performance. The MAEs of RT60 for Var-2, Var-3 and Rec-RIR are close. We further employ the two-tailed Z-test to analyze their differences. Results show that there are no significant statistical differences in RT60 estimation between Rec-RIR and Var-2 as well as Var-3 with p-values $p > 0.999$ and $p \approx 0.306 > 0.05$, respectively. Therefore, the proposed setting is the best among all evaluated settings.

TABLE II
ABLATION STUDY FOR LOSS FUNCTIONS.

Exp. ID	λ_{rvb}	λ_{cln}	RT60 (s)		DRR (dB)	
			MAE \downarrow	MAE \downarrow	MAE \downarrow	MAE \downarrow
Var-1	0.0	0.0	0.077 \pm 0.080		1.056 \pm 0.505	
Var-2	1.0	0.0	0.069\pm0.074		0.899 \pm 0.582	
Var-3	0.0	1.0	0.065\pm0.062		0.960 \pm 0.394	
Rec-RIR	1.0	1.0	0.069\pm0.078		0.684\pm0.402	

V. CONCLUSION

We propose Rec-RIR for blind RIR identification. In Rec-RIR, a DNN that consists of cross-band and narrow-band blocks with auxiliary losses is proposed. Rec-RIR estimates the CTF filter directly by reconstructing the noise-free reverberant speech spectra in the STFT domain. After that, a pseudo intrusive measurement process is employed to convert the CTF filter into RIR. Experimental results show that Rec-RIR attains SOTA estimation of RIR and acoustic parameters.

REFERENCES

- [1] E. Vincent, T. Virtanen, and S. Gannot, *Audio source separation and speech enhancement*. John Wiley & Sons, 2018.
- [2] A. Ratnarajah, I. Ananthabhotla, V. Ithapu *et al.*, “Towards improved room impulse response estimation for speech recognition,” in *ICASSP 2023*. IEEE, 2023, pp. 1–5.
- [3] C. Schissler, R. Mehra, and D. Manocha, “High-order diffraction and diffuse reflections for interactive sound propagation in large environments,” *ACM Transactions on Graphics (TOG)*, vol. 33, no. 4, pp. 1–12, 2014.
- [4] G. Stan, J. Embrechts, and D. Archambeau, “Comparison of different impulse response measurement techniques,” *Journal of the Audio engineering society*, vol. 50, no. 4, pp. 249–262, 2002.
- [5] M. Jalmby, F. Elvander, and T. Van Waterschoot, “Low-rank room impulse response estimation,” *IEEE/ACM Transactions on Audio, Speech, and Language Processing*, vol. 31, pp. 957–969, 2023.
- [6] Y. Lin and D. Lee, “Bayesian regularization and nonnegative deconvolution for room impulse response estimation,” *IEEE Transactions on Signal Processing*, vol. 54, no. 3, pp. 839–847, 2006.
- [7] K. Crammer and D. Lee, “Room impulse response estimation using sparse online prediction and absolute loss,” in *2006 IEEE International Conference on Acoustics Speech and Signal Processing Proceedings*, vol. 3. IEEE, 2006, pp. III–III.
- [8] M. Crocco and A. Del Bue, “Room impulse response estimation by iterative weighted 1 1-norm,” in *EUSIPCO 2015*. IEEE, 2015, pp. 1895–1899.
- [9] C. Steinmetz, V. Ithapu, and P. Calamia, “Filtered noise shaping for time domain room impulse response estimation from reverberant speech,” in *2021 IEEE Workshop on Applications of Signal Processing to Audio and Acoustics*. IEEE, 2021, pp. 221–225.
- [10] Z. Liao, F. Xiong, J. Luo *et al.*, “Blind estimation of room impulse response from monaural reverberant speech with segmental generative neural network,” in *Interspeech 2023*, 2023, pp. 2723–2727.
- [11] R. Talmon, I. Cohen, and S. Gannot, “Relative transfer function identification using convolutional transfer function approximation,” *IEEE Transactions on audio, speech, and language processing*, vol. 17, no. 4, pp. 546–555, 2009.
- [12] J. Lemercier, E. Moliner, S. Welker *et al.*, “Unsupervised blind joint dereverberation and room acoustics estimation with diffusion models,” *IEEE Transactions on Audio, Speech and Language Processing*, vol. 33, pp. 2244–2258, 2025.
- [13] P. Wang, Y. Fang, and X. Li, “Vinp: Variational bayesian inference with neural speech prior for joint asr-effective speech dereverberation and blindrir identification,” *IEEE Transactions on Audio, Speech and Language Processing*, vol. 33, pp. 4387–4399, 2025.
- [14] C. Quan and X. Li, “Spatialnet: Extensively learning spatial information for multichannel joint speech separation, denoising and dereverberation,” *IEEE/ACM Transactions on Audio, Speech, and Language Processing*, vol. 32, pp. 1310–1323, 2024.
- [15] ——, “Multichannel long-term streaming neural speech enhancement for static and moving speakers,” *IEEE Signal Processing Letters*, vol. 31, pp. 2295–2299, 2024.
- [16] N. Shao, R. Zhou, P. Wang *et al.*, “Cleanmel: Mel-spectrogram enhancement for improving both speech quality and asr,” *IEEE Transactions on Audio, Speech and Language Processing*, pp. 1–13, 2025.
- [17] Y. Avargel and I. Cohen, “System identification in the short-time fourier transform domain with crossband filtering,” *IEEE transactions on Audio, Speech, and Language processing*, vol. 15, no. 4, pp. 1305–1319, 2007.
- [18] J. Tang, W. Zhu, and X. Li, “Personal sound zones in the short-time fourier transform domain with relaxed reverberation,” *The Journal of the Acoustical Society of America*, vol. 157, no. 2, pp. 778–796, 2025.
- [19] Z. Wang, G. Wichern, and J. Le Roux, “On the compensation between magnitude and phase in speech separation,” *IEEE Signal Processing Letters*, vol. 28, pp. 2018–2022, 2021.
- [20] A. Farina, “Simultaneous measurement of impulse response and distortion with a swept-sine technique,” in *Audio engineering society convention 108*. Audio Engineering Society, 2000.
- [21] C. Reddy, V. Gopal, R. Cutler *et al.*, “The interspeech 2020 deep noise suppression challenge: Datasets, subjective testing framework, and challenge results,” in *Interspeech 2020*, 2020, pp. 2492–2496.
- [22] C. Valentini-Botinhao, X. Wang, S. Takaki *et al.*, “Investigating rnn-based speech enhancement methods for noise-robust text-to-speech.” in *SSW*, 2016, pp. 146–152.
- [23] J. Richter, Y. Wu, S. Krenn *et al.*, “EARS: An anechoic fullband speech dataset benchmarked for speech enhancement and dereverberation,” in *Interspeech*, 2024, pp. 4873–4877.
- [24] D. Diaz-Guerra, A. Miguel, and J. Beltran, “gpurir: A python library for room impulse response simulation with gpu acceleration,” *Multimedia Tools and Applications*, vol. 80, no. 4, pp. 5653–5671, 2021.
- [25] A. Varga and H. Steeneken, “Assessment for automatic speech recognition: II. noisex-92: A database and an experiment to study the effect of additive noise on speech recognition systems,” *Speech communication*, vol. 12, no. 3, pp. 247–251, 1993.
- [26] K. Kinoshita, M. Delcroix, T. Yoshioka *et al.*, “The reverb challenge: A common evaluation framework for dereverberation and recognition of reverberant speech,” in *2013 IEEE Workshop on Applications of Signal Processing to Audio and Acoustics*. IEEE, 2013, pp. 1–4.
- [27] D. Paul and J. Baker, “The design for the wall street journal-based csr corpus,” in *Speech and Natural Language: Proceedings of a Workshop Held at Harriman, New York, February 23–26, 1992*, 1992.
- [28] J. Eaton, N. Gaubitch, A. Moore *et al.*, “Estimation of room acoustic parameters: The ace challenge,” *IEEE/ACM Transactions on Audio, Speech, and Language Processing*, vol. 24, no. 10, pp. 1681–1693, 2016.
- [29] I. Loshchilov and F. Hutter, “Decoupled weight decay regularization,” in *ICLR*, 2018.
- [30] L. McInnes, J. Healy, N. Saul *et al.*, “Umap: Uniform manifold approximation and projection,” *The Journal of Open Source Software*, vol. 3, no. 29, p. 861, 2018.